Adsorption, mobility, and dimerization of benzaldehyde on Pt(111)

Anton M. H. Rasmussen and Bjørk Hammer

Citation: J. Chem. Phys. **136**, 174706 (2012); doi: 10.1063/1.4707952
View online: http://dx.doi.org/10.1063/1.4707952
View Table of Contents: http://jcp.aip.org/resource/1/JCPSA6/v136/i17
Published by the American Institute of Physics.

Adsorption, mobility, and dimerization of benzaldehyde on Pt(111)

Anton M. H. Rasmussen and Bjørk Hammer[a)]
Interdisciplinary Nanoscience Center (iNANO) and Department of Physics and Astronomy, Aarhus University, DK 8000 Aarhus, Denmark

(Received 22 December 2011; accepted 11 April 2012; published online 4 May 2012)

Building on results for the adsorption of benzene on Pt(111), the adsorption of benzaldehyde is investigated using density functional theory. Benzaldehyde is found to chemisorb preferentially with its aromatic ring in the flat-lying bridge geometry that is also preferred for benzene. Across the investigated geometries, adsorption is homogeneously weakened compared to corresponding benzene geometries. This is found to be true for very different adsorption modes, namely, η^6 and η^8 modes, the latter having metal atoms inserted in the carbonyl bond. Reorientation and diffusion of benzaldehyde is found to have low energy barriers. Aggregation of molecules in dimers bound by aryl C–H···O hydrogen bonds is investigated, and specific configurations are found to be up to 0.15 eV more favorable than optimally configured, separated adsorbates. The binding is significantly stronger than what is found for gas phase dimers, suggesting an enhancing effect of the metal interaction. © *2012 American Institute of Physics*. [http://dx.doi.org/10.1063/1.4707952]

I. INTRODUCTION

Understanding the adsorption of molecules on metal surfaces and the interaction between adsorbates is of key interest in many areas, e.g., catalysis and self-assembly. In the last decade, atomistic insight into these phenomena has emerged based on combining scanning probe microscopy and electronic structure calculations and it is now becoming possible to study larger systems like reactant-modifier complexes in Orito-like reactions.[1] Here, aromatic moieties play a crucial role in the bonding to the surface and their presence has also been suggested to play a role in reaction rate enhancement.[2] Overall the adsorption of aromatic molecules is of fundamental interest and has thus received much attention from both experimental and theoretical[3] investigations. Nonetheless, the adsorption of benzene on various metal surfaces is not yet fully resolved. The added complexity of substituted aromatics makes these less studied than the simpler benzene, but a number of studies do exist, e.g., for ketones[2,4,5] and anisoles.[6–8]

In this paper, we revisit benzene adsorption on Pt(111), and then perform a thorough investigation of the adsorption of benzaldehyde as a model for aromatic ketone reactants.

II. COMPUTATIONAL METHOD

Calculations are performed using density functional theory (DFT) implemented in the GPAW software,[9,10] using the ASE interface.[11] GPAW is based on real space grids and uses the projector augmented wave method.[12,13] The primary parameter to converge with this method is the grid spacing and we find that 0.175 Å is sufficiently fine to obtain reliably optimized geometries and energy differences.

We approximate single molecule adsorption on the Pt(111) surface using a $c(8 \times 4)$ slab, i.e., 16 Pt atoms in each layer. This corresponds to a coverage of $\theta = 0.40$ ($\theta = 1$ being the experimental monolayer saturation coverage) which is lower than in previous studies of benzene.[14,15] Throughout the main paper four layer slabs are used, which matches that used in the work of Morin, Simon, and Sautet,[14] where also six layers were investigated. We estimate that thicker slabs would stabilize adsorbates by up to 0.2 eV, see the Appendix. Calculations are performed using a 2×2 k-point mesh, which is found to be sufficient for 4 layer slabs. Using a denser mesh changes adsorption energies less than 0.04 eV. For dimer calculations we use a $c(12 \times 6)$ slab with 36 atoms in each layer, also using a 2×2 k-point mesh.

The calculation cell is periodic in two directions and terminated with zero-density conditions in the directions perpendicular to the surface. 6 Å of vacuum is used on the bottom of the slab and approximately 8 Å of vacuum is used above the adsorbed molecule. All calculations are non-spin-polarized and performed using the Perdew-Burke-Ernzerhof (PBE) generalized gradient approximation density functional. The slab is setup with a self-consistent lattice constant ($a = 3.98$ Å compared to the experimental value of $a = 3.92$ Å).

The real space grid introduces the so called egg-box effect[16] that causes calculated quantities to depend on the position of atoms relative to the grid points. To minimize this effect, all slab calculations are performed with the bottom layer fixed. During geometry optimization all other coordinates are allowed to relax until all atomic forces are below 0.05 eV/Å.

Geometries used for vibrational analysis are further relaxed to below 0.01 eV/Å, and the Hessian is approximated from the forces of geometries displaced ±0.01 Å in each Cartesian direction. The derivatives of the dipole moment along normal modes are similarly approximated from the displaced geometries. Using a stencil with two additional displaced geometries at ±0.02 Å, has been found to influence neither frequencies nor dipole moments significantly. The square of the dipole derivative component perpendicular to the surface is used for simulated intensities corresponding to

a)Electronic mail: hammer@phys.au.dk.

RAIRS.[17] The same intensities are used for simulating intensities for specular HREELS. Using the more correct expression of Ibach[18] does not change our conclusions but does increase the relative intensity of low frequency modes.

To find minimum energy paths and transition states, we have performed climbing image nudged elastic band calculations.[19]

III. BENZENE

A. Background

Owing to the prototypical nature of benzene, its adsorption has been the subject of a large number of both experimental and theoretical investigations, many concerning the catalytically active platinum (111) surface.[20–28] The adsorption of benzene on Pt(111) is usually interpreted in terms of the eight high symmetry adsorption geometries illustrated in Fig. 1.

STM imaging at low temperatures reveals one primary adsorption geometry of twofold rotational symmetry, a secondary of threefold rotational symmetry (occurring in two orientations), as well as a higher symmetry geometry occurring only near defects and other adsorbates.[22] RAIRS experiments display dependency on both coverage and temperature, and indicate three distinct binding environments,[25] one of these having a spectrum very similar to that of the gas phase molecule. NEXAFS experiments indicate out of plane distortions,[24] which is supported by diffuse LEED experiments, that also indicate twofold rotational symmetry.[21] Recent HREELS results indicate lower symmetry than C_{2v} or multiple adsorption sites.[29] The most recent density functional theory studies[14,30–32] agree upon the so-called bridge30 geometry (see Fig. 1) as the most energetically favorable, followed by the so-called fcc0 and hcp0 geometries. Simulated vibrational spectra for the bridge30 agree reasonably well with most RAIRS and HREELS experiments, but a secondary site is usually assumed to replicate all observed frequencies. From theoretical investigations, the binding of benzene to the platinum has been suggested to involve donation and back-donation between the molecular HOMO-LUMO orbitals and the platinum *d*-states.[31] The overall charge transfer was found to leave the molecule slightly positive, and the interaction with the metal *d*-states leads to a partial rehybridization of the carbon orbitals from sp^2 towards sp^3 character, which facilitates the experimentally observed distortion where the C–H bonds are tilted away from the surface. Furthermore, the C–C bonds are elongated to various degree, depending on the investigated adsorption geometry.

The adsorption strength has been probed using temperature programmed desorption, which displays two desorption peaks,[20] corresponding to desorption energies of 1.34 eV at low coverage and 0.91 eV at higher coverage (1.21 eV and 0.85 eV in a later study[23]). More recently the heat of adsorption of benzene on Pt(111) has been measured by calorimetry showing a much stronger adsorption energy of −1.90 eV at the coverage of $\theta = 0.40$ used in this work.[26]

Calculated adsorption energies depend on calculation methods, but in general agree better with the older TPD studies than with the more recent calorimetric measurements. This apparent underestimation of the binding by DFT is consistent across larger heterocyclic aromatic species, and has been attributed to the inadequate description of dispersion within the applied DFT approximations.[33] Similarly, the adsorption energy of benzene on nickel is found to increase, when using the more accurate correlation of the RPA method[34] instead of PBE DFT.

B. Results and discussion

We first consider the eight high symmetry, flat-lying benzene geometries illustrated in Fig. 1: Four sites combined with two orientations of the molecule. The adsorption energies resulting from our calculations are compared with results from the literature in Table I.

In agreement with previous theoretical studies,[14,30–32] we find that the preferred binding geometry for benzene is bridge30, which is illustrated in Fig. 1. In this geometry, the two apical carbons ((a) in Fig. 1) have their CH bonds tilted 34° from horizontal, while the bridging carbons ((b) in the figure) have their CH bond tilted 18°. The C–C bonds are elongated to 1.473 Å and 1.435 Å compared to the calculated gas phase value of 1.397 Å. Our calculations give an adsorption energy of −1.19 eV, which is a somewhat weaker binding than

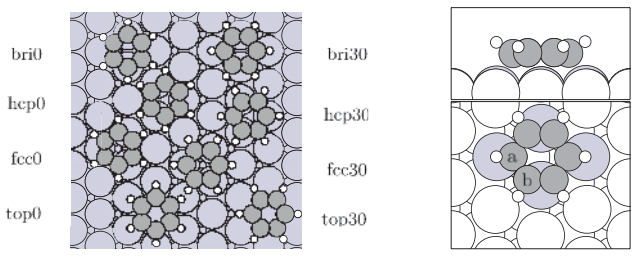

FIG. 1. (Left) Schematic geometries for the investigated benzene adsorption sites. The naming scheme indicates the benzene center position and the angle between C–C bonds and the Pt–Pt nearest neighbor direction. (Right) The energetically favorable bridge30 configuration. The apical carbon (a) is interacting with its own metal atoms, while the bridging carbon (b) is sharing a platinum atom.

TABLE I. Calculated adsorption energies (eV) for benzene on Pt(111).

	Present work	Ref. 14		Ref. 30
XC approx.	PBE	PW91		BP86
Pt(111) model	4 l. slab	4 l. slab	6 l. slab	Pt_{22} cluster
Coverage	0.4	0.7	0.7	...
bri30	−1.19	−0.90	−1.04	−1.06
bri0	−0.59[a]	−0.30	−0.45	−0.68
hcp30	−0.51[a]	−0.33	−0.41	−0.53
hcp0	−0.96	−0.67	−0.76	−0.73
fcc30	−0.42[a]	−0.27		−0.56
fcc0	−0.91	−0.61		−0.67
top30	Unstable	Unstable		
top0	0.19	Unstable		
top0 (vacancy)	−1.96			

[a]Found to be saddle points.

the heat of adsorption measured by calorimetry: −1.90 eV.[26] We estimate that approximately 0.2 eV of this deviation may be attributed to an insufficient number of layers in our slab, as the four layers show the weakest binding of all investigated slabs.

The second most stable geometry has the benzene ring centered on the 3-fold hollow hcp site, C–C bonds rotated 0° relative to the platinum rows. This geometry is found to be 0.2 eV less stable compared to the bridge30 configuration. The hollow fcc site is found to be further 0.05 eV less stable, which is consistent with the literature. This small asymmetry between fcc and hcp adsorption strength shows that the second metal layer has a small but non-zero influence on the adsorption. The bridge0 geometry and the even less stable hollow30 geometry are found to be saddle points, from where the molecule may rotate with no barrier to the more stable bridge30 and hollow0 geometries, respectively. Finally, adsorption centered ontop platinum atoms is found to be stable (unstable) for the 0° (30°) orientation but energetically very unfavorable.

Adsorption at defect sites has been suggested as an explanation for STM observation with a high degree of rotational symmetry,[22] we find that adsorption of benzene above a surface vacancy (ontop0 geometry with the central Pt atom removed) gives an adsorption energy of −1.96 eV, 0.77 eV more stable than the preferred geometry on the clean slab. The stronger interaction is reflected by the C–C bonds being further elongated to alternating 1.490 Å and 1.493 Å, and increased CH tilting of 41°.

We calculate the formation energy of the Pt(111) surface vacancy to be 1.16 eV when the excess atom is considered to go to the bulk. This number might need correction[35] since the PBE functional is known to underestimate the surface and cohesive energies of platinum,[36] thus underestimating the formation energy of the vacancy. However, even at this level of theory it is unfavorable to form a vacancy upon adsorption (−1.96 eV + 1.16 eV = −0.80 eV) compared to the bridge30 geometry, suggesting that only already existing vacancies are adsorption sites.

1. Vibrational analysis

In Fig. 2, we present a comparison of recent HREELS measurements[29] to simulated spectra for the most stable geometries, bridge30, hcp0, and fcc0 (frequencies are tabulated in the supplementary material[37]). All observed losses (vertical lines) are matched closely by calculated frequencies (triangles) for the bridge30 configuration. The CH stretching modes around 3000 cm^{-1} are overestimated, most likely due to anharmonicity not being considered. Intensities are less closely matched; a number of modes appear too weak in the calculations when comparing to the experimental spectrum, which could be the result of non-dipole scattering in the experiment.

In Figure 3, sections of the calculated spectra are shown along with RAIRS observations[25] indicated by vertical lines. As for the HREELS observations, we find that the bridge30 site is sufficient to explain the room temperature observations (full lines). However, the observation of coverage and temperature dependent intensity ratios of the losses at 820 cm^{-1}, 830 cm^{-1}, and 900 cm^{-1} was interpreted as evidence of multiple site occupancy, with the band at 900 cm^{-1} representing the bridge30 site and the bands at 820 cm^{-1} and 830 cm^{-1} representing the hollow sites. This latter interpretation is however not easily reconciled with the calculated wavenumber of the single high activity mode of the hcp0(fcc0) geometry at 803 cm^{-1} (778 cm^{-1}), which appears too far from the observed losses.

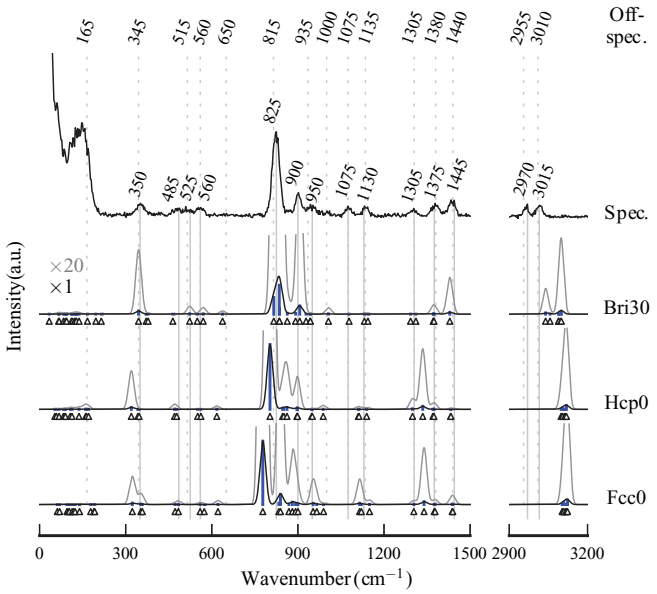

FIG. 2. Simulated specular HREELS spectra (three lowest spectra) compared to recent experimental data taken at specular angle, 300 K, and 1 L (top spectrum, full vertical lines) and taken at off-specular angle, 300 K, 6.5 L (dashed vertical lines). The simulated spectra are calculated by folding calculated intensities with a Lorentzian.

A possible explanation for the variations in intensities can emerge from assigning the two losses observed at 820 cm^{-1} and 830 cm^{-1} to the three computed normal modes at: 816 cm^{-1} (bending of the hcp-end apical CH), 835 cm^{-1} (bending of all six CH with ring breathing), and 836 cm^{-1} (bending of the fcc-end apical CH). Interaction between adsorbates may then have different impact on the three losses, allowing for coverage dependent intensity ratios. Such effects

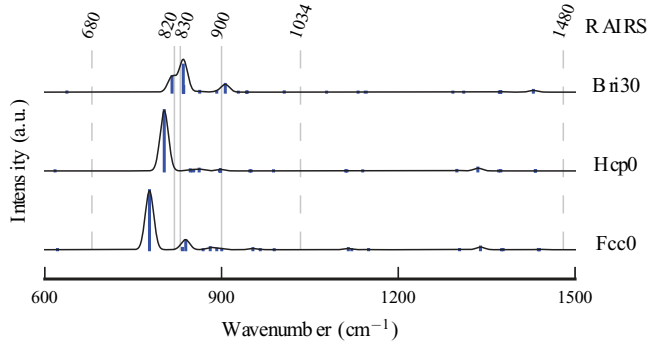

FIG. 3. Simulated RAIRS intensities and spectra for the three most stable adsorption sites. For comparison, vertical lines indicate experimentally observed losses. Dashed vertical lines represent losses that disappear upon heating. The simulated spectra are calculated by folding calculated intensities with a Lorentzian.

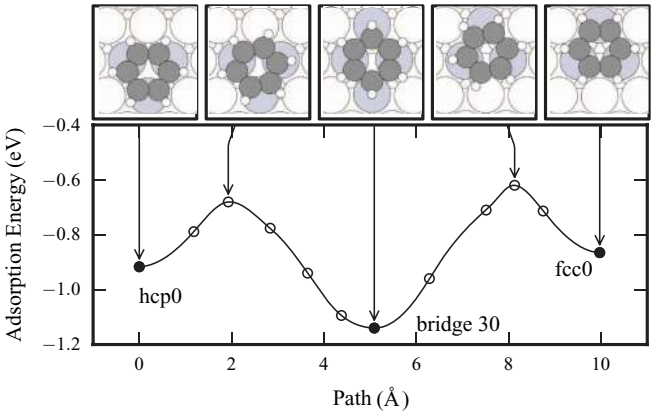

FIG. 4. Pathway and energy profile for diffusion between the most stable benzene sites.

are also observed in the measurements of Demers-Carpentier and McBreen,[29] where the intensity ratio of the two CH stretching losses around 3000 cm^{-1} is seen to vary with coverage. Our calculations show that these two peaks consist of apical CH stretching and bridging CH stretching, respectively, allowing for different coverage dependencies in their activities too.

2. Mobility

Diffusion of the adsorbed aromatic molecule across the surface is assumed to take place with the molecule in flat-lying geometries. The minimum energy path for diffusion between hcp0 and bridge30 is found to keep two carbon atoms of the phenyl bonded to one platinum atom, which then acts as a hinge for benzene to rotate around. The same mechanism is also found for the bridge30 to fcc0 transition. Combining two such transitions, as shown in Fig. 4, the entire metal surface may be reached by the diffusing molecule. The barriers for connecting neighboring bridge30 sites is approximately 0.6 eV.

IV. BENZALDEHYDE

The effect of side groups on the adsorption of benzene has been studied but much less than benzene itself. Substituting on a single benzene adsorption geometry, Tan *et al.* found that anisole ($CH_3OC_6H_5$) on Pt(111) adsorbs somewhat weaker than benzene, and that the molecule gained a slight positive charge upon adsorption.[6] The distorted geometry of benzene was retained, leading to a decoupling of the aromatic system and the methoxy group. Derivatives of anisole were investigated by Bonalumi *et al.*[8] Their work revealed a further weakening of the adsorption upon substitution, and it was concluded that electron withdrawing substituents weaken the bond by recalling electron density from the metal surface.

When adding functionality to benzene, the symmetry is lowered and more adsorption geometries are possible. We use the eight high symmetry geometries of Fig. 1 for the aromatic ring as a starting point. Disregarding molecular distortion, as well as interactions between the aldehyde group and second layer Pt atoms, 15 unique combinations of site and rotation are possible. Besides geometry of the ring and the various substitutions, one must also consider possible interactions between the side group and the metal. After relaxation, this leads to 17 stable adsorption geometries, these are depicted in Fig. 5. Their adsorption energies and their relation to the adsorption energies of benzene in corresponding geometries are illustrated in Fig. 6.

From the latter figure, it is clear that the general effect of adding the side group is a lower stability of the chemisorbed state by up to 0.2 eV, regardless of the orientation of the aromatic ring. Although not visible from Fig. 6 this also applies to benzaldehyde adsorbed on a Pt vacancy, N in Fig. 5. Thereby, the preference for the bridge30 ring geometry is preserved.

Focusing then on the bridge30 geometry for the ring, there are a number of possibilities when substituting the aldehyde. On the bridge30 benzene two different carbon species are present: two apical carbons with pronounced hydrogen tilting and four bridging carbons (see Fig. 1).

Substituting on one apical carbon or the other differs only in second layer platinum geometry, resulting in energetic differences below 0.05 eV, while mirroring the aldehyde group yields no influence on binding. Thus, only one apical configuration is considered, denoted **A**. The relaxed geometry is illustrated in Fig. 5. It has the aldehyde group tilted away from the surface at an angle of 31°, slightly less than the 34° of the apical hydrogen of adsorbed benzene.

When substituting the aldehyde group on the bridging carbon, mirroring the aldehyde group leads to distinct geometries: **B** and **C**. The mirror plane of the aldehyde is not a mirror symmetry plane of the platinum surface, thus different interactions with the surface are possible for the two configurations. **B** has, like **A**, the substituent group pointing away from the surface, while **C** can have the aldehyde group either tilted away or parallel to the surface. The tilt angles are found to be 23° and 21°, compared to the benzene bridging CH bend of 18°. In the case of parallel adsorption, the carbonyl interacts with the underlying platinum atoms, whereby the CO bond length is increased from the gas phase value of 1.23 Å to 1.32 Å, indicating partial breaking of the carbonyl double bond. We denote configurations involving such interactions with an asterisk, i.e., **C***. The two different modes **C** and **C*** are separated by only 0.05 eV, which requires a delicate balancing of phenyl-Pt interactions, the CO-Pt interactions, and the cost of distorting the molecule.

To analyze the energetics of the adsorption modes, we consider the adsorption energy as the sum of three terms

$$E_{\mathrm{ad}} = E_{\mathrm{mol}} + E_{\mathrm{surf}} + E_{\mathrm{int}}, \tag{1}$$

E_{mol} is a cost due to molecular distortion, E_{surf} is a cost due to surface distortion, and finally E_{int} is the interaction energy of the distorted compounds. The distortion energies are calculated as the energy of the molecule (surface) distorted as in the compound system, subtracted the energy of the isolated molecule (surface) in its optimized geometry. The interaction energy is then defined as the adsorption energy minus the two distortion energies. E_{ad}, E_{mol}, and E_{surf} are thus directly calculated while E_{int} takes the value necessary to fulfill Eq. (1). The numbers for **A**, **B**, **C**, and **C*** are tabulated in

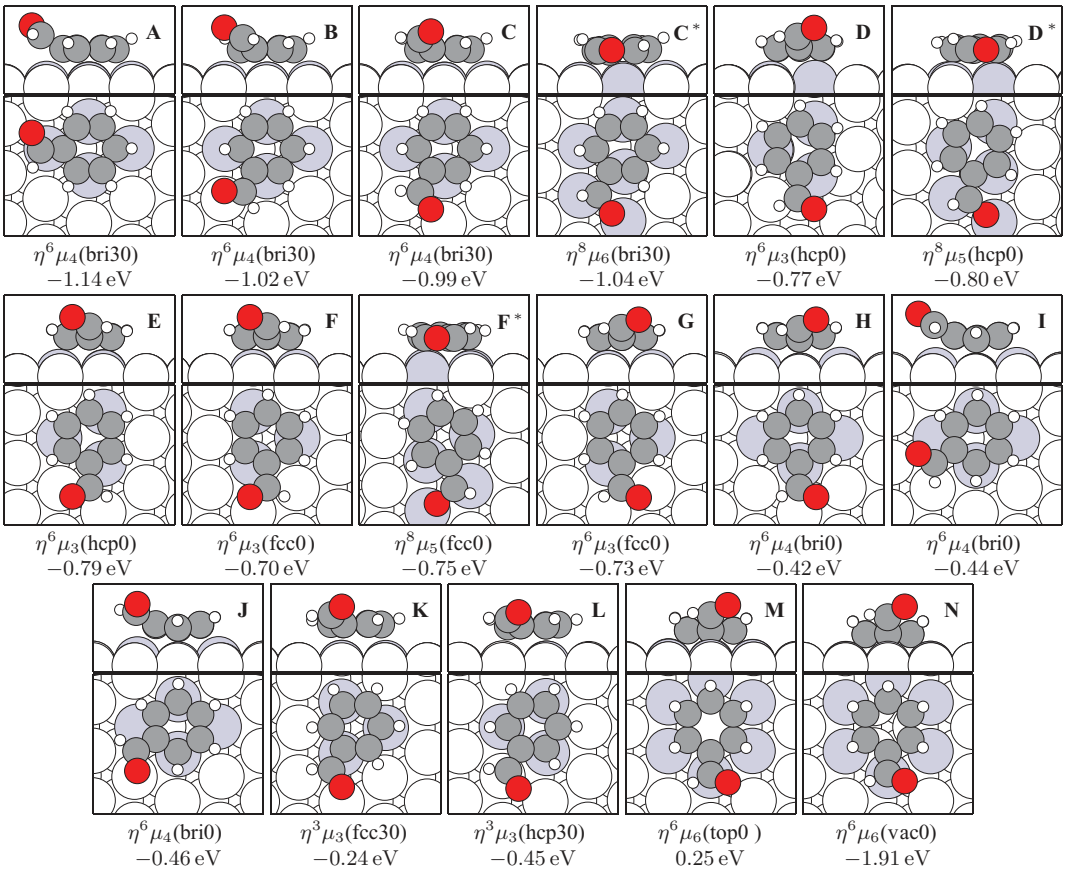

FIG. 5. Stationary geometries of benzaldehyde on Pt(111). The notation $\eta^n\mu_m(z)$ indicates bonding between n atoms in the molecule and m Pt atoms, phenyl centered on a Pt site of type z. Pt atoms within 2.5 Å of carbon atoms are shaded.

Table II. They reflect that the CO-Pt interaction of **C*** yields a substantially increased interaction energy at the cost of expensive molecular distortion, which we assign primarily to C–O bond elongation. Curiously, the 31° bent molecule of **A** has a lower distortion energy than the molecules of the **B** and **C** that are bent 23° and 21°. This suggests that E_{mol} is not explainable solely by the magnitude of the out of plane distortion.

To further investigate the bonding in the **C*** geometry, we resort to the induced electron density, defined as the electron density of the surface-molecule compound, subtracted the densities of the isolated surface and the isolated molecule (both distorted as in the compound system). This quantity reflects the adjustment of the electronic density of separated systems when they are brought together, an adjustment responsible for the interaction energy E_{int}. Slices along several planes through the induced density of the **C*** configuration are shown in Fig. 7. These illustrate the binding of the carbonyl C and O to surface platinum atoms. For both platinum atoms, a depletion of a region resembling the metal d_{z^2} orbitals is observed along with accumulation of charge where atomic spheres of C and O meet those of platinum.

It is interesting to note that similar energetics with and without metal insertion in the carbonyl bond also results when substituting on the hollow0 geometries: **D/D*** are separated by only 0.03 eV and **F/F*** by 0.05 eV. From a thermodynamic point of view, both adsorption modes are then expected to occur, a fact of importance to reactivity[5] and selectivity[38–41] in hydrogenation reactions.

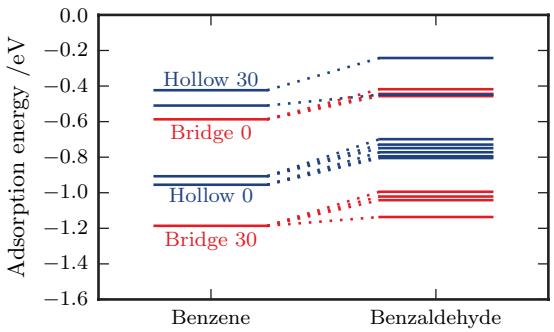

FIG. 6. Adsorption energies for the investigated benzene adsorption sites, along with adsorption energies for aldehyde substitutions on these geometries.

TABLE II. Adsorption energy and components hereof (eV) for selected geometries.

	mode	E_{ad}	E_{mol}	E_{surf}	E_{int}
Benzene bri30	$\eta^6\mu_4$	−1.19	1.57	0.34	−3.09
Benzaldehyde **A**	$\eta^6\mu_4$	−1.14	1.45	0.33	−2.92
Benzaldehyde **B**	$\eta^6\mu_4$	−1.02	1.68	0.40	−3.09
Benzaldehyde **C**	$\eta^6\mu_4$	−0.99	1.65	0.39	−3.03
Benzaldehyde **C***	$\eta^8\mu_6$	−1.04	2.36	0.37	−3.77

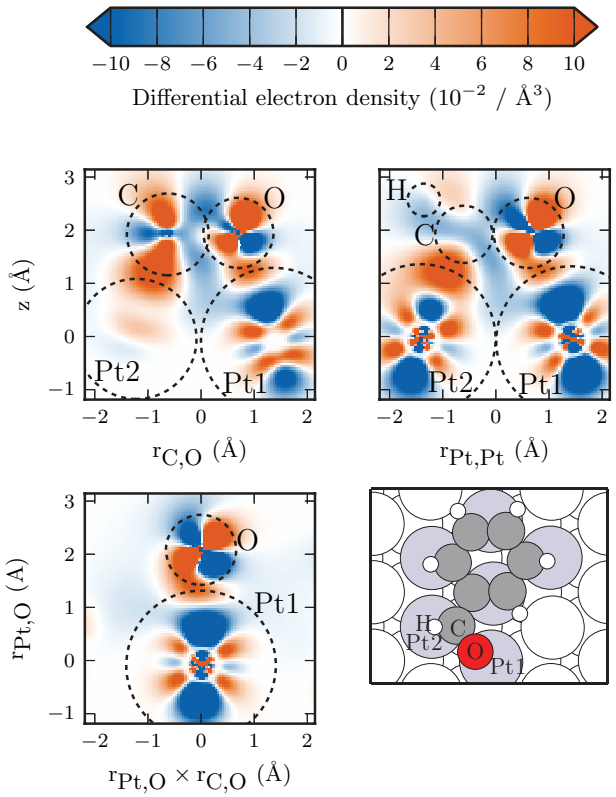

FIG. 7. Slices through the differential density of **C***. Dashed circles indicate intersections of the slicing plane with atom centered spheres of covalent radii.

A. Mobility

We have investigated reorientation of the CHO moiety with the aromatic ring remaining in the same site, and movement of the aromatic ring from one site to another.

Rotation of the CHO around the CC bond between the substituent and the phenyl, transforms the apical substituted **A** configuration to its own mirror image. The bridge substituted configurations **B** and **C** are connected by a corresponding rotation, while **C** and **C*** are connected through the tilting of the CHO moiety. Minimum energy paths for these transformations make up Fig. 8. Only barriers lower than 0.5 eV are present.

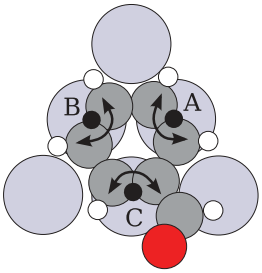

FIG. 9. From the threefold coordinated **D** configuration, three different C–Pt di-σ bonds (A, B, C) may act as hinges for rotating into the corresponding geometries **A**, **B**, **C** at the three neighboring fourfold sites.

Rotation of the CHO moiety is seen to have comparable barriers when the oxygen atom rotates away from the surface or near the surface. In the case of **C** to **B** rotation with oxygen pointing towards the metal, some O–Pt attraction is observed near the transition state, creating a shoulder in the energy curve. This interaction also shows in a slight elongation of the C–O bond at this rotational angle. Interestingly, a very low barrier is observed between the states with and without carbonyl-Pt interaction, **C*** and **C**.

Moving to the diffusion of benzaldehyde, an inspection of the adsorption configurations reveals that from any configuration, **A**, **B**, **C**, or **C***, a similar neighboring configuration can be reached via an intermediate **D** configuration. The diffusion occurs as the hinging mechanism already discussed for benzene diffusion from bridge30 via hcp0/fcc0 to bridge30. Because of symmetry, we need only consider the second part of the diffusion process, i.e., from **D** to an **A**, **B**, or **C/C*** configuration. This is illustrated in Fig. 9 that depicts how the resulting configuration becomes **A**, **B**, or **C/C***, depending on which Pt atom is chosen for the hinging.

In Figure 10, we show barriers for the diffusion from **D** to **A**, **B**, **C** with a barrier of ≈0.2 eV. The reverse process back to **D** has a barrier of around 0.6 eV, and may occur using one of two metal atoms as a hinge. The choice of hinging atom

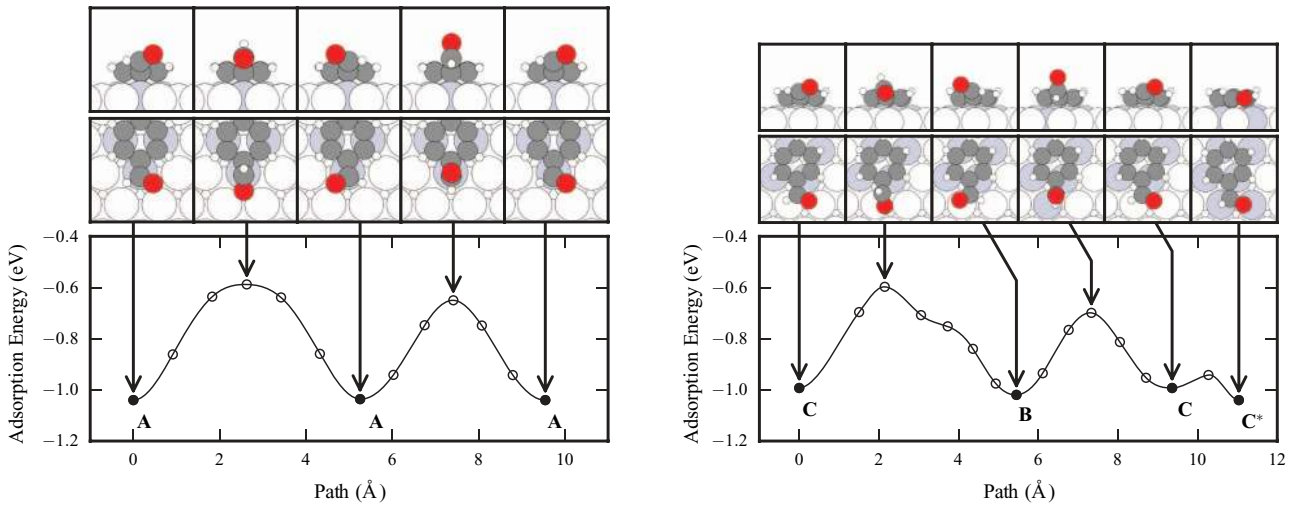

FIG. 8. Pathways and energy profiles for reorientation of aldehyde group when substituted on the apical carbon (left) and on the bridging carbon (right).

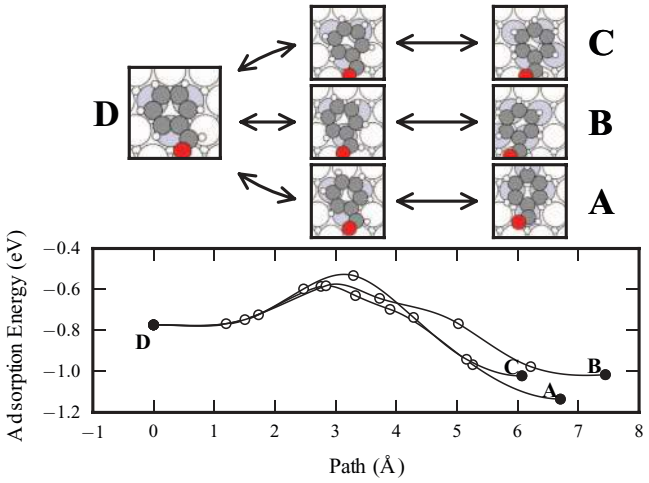

FIG. 10. Pathways and energy profiles for diffusing from the **D** geometry to the **A**, **B**, and **C** configurations.

determines whether the **D** is reached at its original orientation or rotated 60°.

Thus, only barriers below approximately 0.6 eV connect the **A**,**B**, **C**, **C***, and **D** benzaldehyde geometries. Based on transition state theory, the adsorbed molecules are then able to diffuse and reorient at rates faster than $De^{-0.6\text{eV}/kT} \approx 100s^{-1}$, assuming a prefactor of $D = 10^{13}s^{-1}$ and room temperature.

B. Dimer formation

Having shown in Sec. IV A that the barriers for single benzaldehyde molecule diffusion and reorientation are low, high mobility is expected at moderate temperatures. Thus, we now turn to investigate how the molecules may assemble into dimers bonded by CH···O hydrogen bonds. Such bonds have been observed experimentally for other similar molecules,[42] and are believed to be a determining factor for both rate and selectivity in catalytic hydrogenation reactions.[2]

A number of configurations are investigated, namely, pairs of the most stable monomer configurations, the relaxed geometries are shown in Figs. 11 and 12 (larger top views are available in the supplementary material[37]).

The energetic cost of placing two molecules next to each other is found to be vanishing (compare **AA3** with **2A** in Fig. 11), thus ruling out significant interactions between the aromatic rings. Once the molecules are next to each other (**AA3**), one or two hydrogen CH···O bonds may be established by rotating the aldehyde groups one by one (**AA2** and **AA1**). Using two separated molecules in the most stable **A** geometry as reference (**2A**), we find that the **AA1** dimer has a relative energy of −0.14 eV, with each hydrogen bond contributing approximately equally. The **BB** dimer has slightly stronger hydrogen bond interactions, but as a consequence of being composed of less stable monomer geometries it has an energy very similar to the reference system **2A**. Interestingly, the **CC** dimer relaxes to the **C*C*** dimer shown in Fig. 12, indicating that the small barrier observed for the **C** to **C*** transition, is lowered by the nearby aromatic. In the same figure, a number of less symmetric dimers are also depicted.

Most of the investigated dimers are found, by visual inspection, to have two or more plausible CH···O hydrogen bonds, while, e.g., the stronger bonded asymmetric **AA4** dimer is stabilized by only one bond. To estimate the strength of each hydrogen bond, we compare the dimer energies to that of the separated constituents by defining the average energy per hydrogen bond as

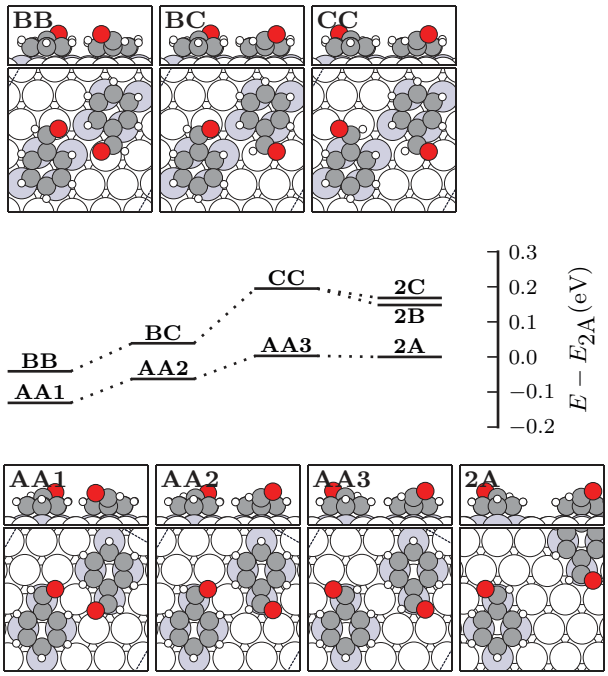

FIG. 11. Investigated dimer configurations composed of oppositely oriented monomers. The energy of two separated molecules **2A** is used as the reference on the energy scale.

$$E_{\text{HB}} = \frac{E_{\text{dimer}} - E_{\text{sep}}}{N_{\text{HB}}}, \tag{2}$$

where N_{HB} is the estimated number of hydrogen bonds.

In Table III, we list dimer energies and energies per hydrogen bond, along with bond distances and angles for the possible hydrogen bonds. The geometric parameters show quite some variation due to the constraints imposed by the

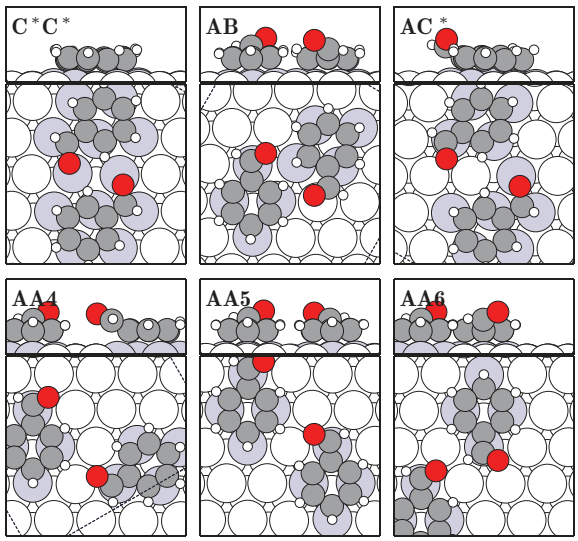

FIG. 12. Dimer configurations complementing the symmetric dimers in Fig. 11.

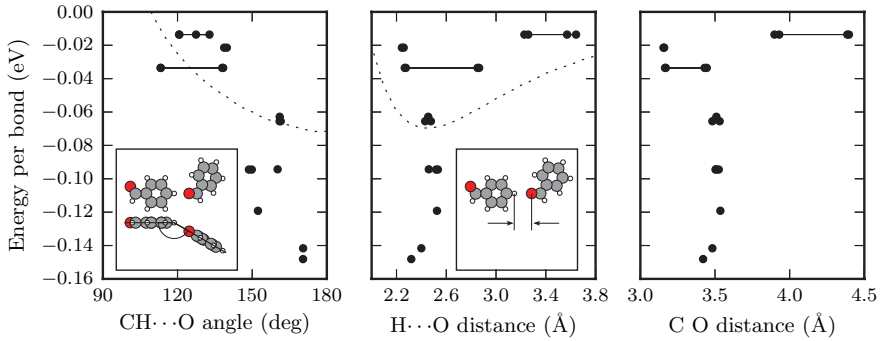

FIG. 13. The hydrogen bond energies of the dimers versus geometric parameters of these dimers are shown with black dots. In case of several bonds in one dimer, the dots representing these bonds are connected with horizontal lines. For comparison, the dashed lines show binding energies of the gas phase dimers shown in the insets. The gas phase geometries are relaxed with constraints in order to probe the dependency of the interaction strength on specific geometric parameters of the CH···O bond. For the CH···O angle, the geometry is optimized with the H···O distance fixed, and the two molecules constrained to two bisecting planes. When probing the dependency on H···O distance, all atoms are restricted to one plane, the bonding H and O are fixed, and the O=C direction is fixed.

strong metal-molecule interaction. This is generally in agreement with statistical analysis of Steiner that indicates that CH···O bonds are found with a wide range of bond lengths and angles, although a tendency for linear bonds is seen, especially for shorter bonds.[43] The **AA6**, **AA4**, and **BC** hydrogen bonds are relatively strong when comparing to reported typical CH···O strengths of 0.04 eV to 0.09 eV.[43,44] The strengths of the hydrogen bonds in the adsorbed dimers may be compared to those of gas phase benzaldehyde dimers. This is done in Fig. 13, where the bond strengths as a function of CH···O angle and O···H distance for adsorbed dimers (dots) and gas phase dimers (dashed lines) are compared. For the gas phase calculations, only the relevant geometric parameter have been fixed. We observe that bond angles near 180° correlates with large bond strength E_{HB} and that the bonds with significant binding have O···H distances between 2.2 Å and 2.6 Å. Weak bonds are however also found in this range of O···H distances, leading us to conclude that the angle is the determining factor for the bond strength. The strongest bond between adsorbed molecules is approximately twice that of the optimal gas phase geometry, and is very close to linear, evidencing a favorable effect of the interaction between the metal and the phenyl. This stronger binding agrees with the suggestion of Lavoie and McBreen that aryl C–H···O=C bonding on Pt(111) is enhanced by electron transfer from aromatic carbon to metal.[45] A similar activation effect has been predicted for aryl C–H, when electron withdrawing substituents are present.[46,47]

TABLE III. Energetics of the investigated dimers and parameters for the considered CH···O hydrogen bonds.

	$E - E_{2\mathbf{A}}$ (eV)	E_{HB} (eV)	d_{OH} (Å)	θ_{CHO} (deg)
AA1	−0.13	−0.07	2.45	162
			2.42	161
AA2	−0.06	−0.06	2.46	161
AA3	0.00	…	…	…
BB	−0.04	−0.09	2.53	150
			2.52	149
BC	0.04	−0.12[a]	2.53	152
CC	0.19	…	…	…
C*C*	−0.04	−0.02	2.26	139
			2.24	140
AB	−0.06	−0.03[b]	2.27	138
			2.86	113
			2.28	138
			2.85	113
AC*	−0.05	−0.01[b]	3.26	121
			3.23	121
			3.57	133
			3.64	127
AA4	−0.14	−0.14	2.40	171
AA5	−0.09	−0.09	2.46	160
AA6	−0.15	−0.15	2.32	170

[a]Using $E_{\mathrm{sep}} = (E_{2\mathbf{C}} + E_{2\mathbf{B}})/2$.
[b]Using $E_{\mathrm{sep}} = (E_{2\mathbf{A}} + E_{2\mathbf{X}})/2$.

V. CONCLUSIONS

Using the real space grid DFT code GPAW, we find a good correspondence between calculated and experimental vibrational spectra for adsorbed benzene. The calculated vibrational spectra display sensitivity to the symmetry of the second metal layer, and the primary adsorption site is able to account for all observed losses. In line with previous work, we calculate too weak benzene adsorption on the defect free Pt(111) surface when comparing to calorimetric experiments. This may partly be explained by too few platinum layers being used in calculations, but is probably mostly missing correlation effects in the applied DFT approximation. We add that adsorption directly above an existing surface vacancy is calculated to be energetically very favorable.

Benzaldehyde adsorption is found to be largely dominated by the interaction between the aromatic ring and the platinum surface. Thus, the adsorption geometries are very similar to those of benzene, though benzaldehyde is up to 0.2 eV weaker bonded. The weakening is attributed to increased energetic cost of molecular distortion upon adsorption. In specific geometries, the carbonyl is able to interact with the metal surface, and in these geometries the carbonyl double bond is opened partly by interactions with metal atoms. The adsorption energies of these geometries are found to be remarkably similar to those of modes having the

TABLE IV. Convergence of adsorption energies (eV) for the **C** and **C*** benzaldehyde geometries.

	C*			**C**		
k-points	2 × 2	3 × 3	4 × 4	2 × 2	3 × 3	4 × 4
2 layers	−1.70	−1.59	...	−1.45	−1.35	...
3 layers	−1.72	−1.55	−1.54	−1.46	−1.31	−1.32
4 layers	−1.04	−1.01	−1.02	−0.99	−0.95	−0.97
5 layers	−1.35	−1.26	−1.23	−1.17	−1.12	−1.09
6 layers	−1.21	−1.14	...	−1.13	−1.04	...
7 layers	−1.25	...	...	−1.10	...	...

aldehyde group tilted away from the surface. This is caused by a delicate balance between the cost of carbonyl bond weakening and carbonyl-metal interaction, as well as competition between carbonyl-metal and phenyl-metal interactions.

We find that C–H· · ·O stabilized dimers of adsorbed benzaldehyde are up to 0.15 eV more stable than separated adsorbates in optimal geometries. The strength of the hydrogen bonds is enhanced significantly compared to the gas phase, and a stronger preference for linear hydrogen bonds are observed. Furthermore, the presence of a neighboring aromatic ring is found to stabilize the carbonyl-metal bond slightly.

ACKNOWLEDGMENTS

This research was supported by grants from the Danish Research Councils, The Lundbeck Foundation, and the Danish Center for Scientific Computing.

APPENDIX: CONVERGENCE OF ADSORPTION ENERGIES

Slabs of two to seven layers have been investigated. Results from this convergence test are shown in Table IV for two different benzaldehyde adsorption geometries. We find that adsorption energies show a strong dependency on the number of layers, with two and three layers displaying the strongest binding and four layers displaying the weakest binding. This variation is in line with prior slab calculations[14] and previously reported cluster size dependency,[32] but contradicts the findings of Gao, Zheng, and Jiang.[48] Nonetheless, the dependency on slab thickness is found to be rather independent from binding geometry. Thus, the ordering of binding geometries by energy can be trusted, even though the magnitude of adsorption energies is not fully converged with respect to the number of layers.

[1] V. Demers-Carpentier, G. Goubert, F. Masini, R. Lafleur-Lambert, Y. Dong, S. Lavoie, G. Mahieu, J. Boukouvalas, H. Gao, A. M.H. Rasmussen, L. Ferrighi, Y. Pan, B. Hammer, and P. H. McBreen, Science **334**, 776 (2011).
[2] M.-A. Laliberté, S. Lavoie, B. Hammer, G. Mahieu, and P. H. McBreen, J. Am. Chem. Soc. **130**, 5386 (2008).
[3] S. J. Jenkins, Proc. R. Soc. A **465**, 2949 (2009).
[4] A. Vargas, J. Catal. **222**, 439 (2004).
[5] A. Vargas, S. Reimann, S. Diezi, T. Mallat, and A. Baiker, J. Mol. Catal. A: Chem. **282**, 1 (2008).
[6] Y. Tan, S. Khatua, S. Jenkins, J. Yu, J. Spencer, and D. King, Surf. Sci. **589**, 173 (2005).
[7] N. Bonalumi, A. Vargas, D. Ferri, T. Burgi, T. Mallat, and A. Baiker, J. Am. Chem. Soc. **127**, 8467 (2005).
[8] N. Bonalumi, A. Vargas, D. Ferri, and A. Baiker, J. Phys. Chem. B **110**, 9956 (2006).
[9] J. J. Mortensen, L. B. Hansen, and K. W. Jacobsen, Phys. Rev. B **71**, 035109 (2005).
[10] J. Enkovaara, C. Rostgaard, J. J. Mortensen, J. Chen, M. Dułak, L. Ferrighi, J. Gavnholt, C. Glinsvad, V. Haikola, H. A. Hansen, H. H. Kristoffersen, M. Kuisma, A. H. Larsen, L. Lehtovaara, M. Ljungberg, O. Lopez-Acevedo, P. G. Moses, J. Ojanen, T. Olsen, V. Petzold, N. A. Romero, J. Stausholm-Møller, M. Strange, G. A. Tritsaris, M. Vanin, M. Walter, B. Hammer, H. Häkkinen, G. K.H. Madsen, R. M. Nieminen, J. K. Nørskov, M. Puska, T. T. Rantala, J. Schiøtz, K. S. Thygesen, and K. W. Jacobsen, J. Phys.: Condens. Matter **22**, 253202 (2010).
[11] S. R. Bahn and K. W. Jacobsen, Comput. Sci. Eng. **4**, 56 (2002).
[12] P. E. Blöchl, Phys. Rev. B **50**, 17953 (1994).
[13] P. E. Blöchl, C. J. Först, and J. Schimpl, e-print arXiv:cond-mat/0201015.
[14] C. Morin, D. Simon, and P. Sautet, J. Phys. Chem. B **107**, 2995 (2003).
[15] C. Morin, D. Simon, and P. Sautet, J. Phys. Chem. B **108**, 12084 (2004).
[16] F. Nogueira, A. Castro, and M. Marques, *A Primer in Density Functional Theory*, Lecture Notes in Physics Vol. 620, edited by C. Fiolhais, F. Nogueira, and M. A. L. Marques (Springer, Berlin, 2003), Chap. 6, pp. 218–256.
[17] R. F. Aroca, D. J. Ross, and C. Domingo, Appl. Spectrosc. **58**, 324A–338A (2004).
[18] H. Ibach and D. L. Mills, *Electron Energy Loss Spectroscopy and Surface Vibrations* (Academic, 1982).
[19] G. Henkelman, B. P. Uberuaga, and H. Jónsson, J. Chem. Phys. **113**, 9901 (2000).
[20] J. M. Campbell, S. Seimanides, and C. T. Campbell, J. Phys. Chem. **93**, 815 (1989).
[21] A. Wander, G. Held, R. Hwang, G. Blackman, M. Xu, P. Deandres, M. Vanhove, and G. Somorjai, Surf. Sci. **249**, 21 (1991).
[22] P. S. Weiss and D. M. Eigler, Phys. Rev. Lett. **71**, 3139 (1993).
[23] C. Xu, Y. L. Tsai, and B. E. Koel, J. Phys. Chem. **98**, 585 (1994).
[24] C. Mainka, P. Bagus, A. Schertel, T. Strunskus, M. Grunze, and C. Woll, Surf. Sci. **341**, L1055 (1995).
[25] S. Haq and D. A. King, J. Phys. Chem. **100**, 16957 (1996).
[26] H. Ihm, H. M. Ajo, J. M. Gottfried, P. Bera, and C. T. Campbell, J. Phys. Chem. B **108**, 14627 (2004).
[27] K. M. Bratlie, M. O. Montano, L. D. Flores, M. Paajanen, and G. A. Somorjai, J. Am. Chem. Soc. **128**, 12810 (2006).
[28] K. M. Bratlie, H. Lee, K. Komvopoulos, P. Yang, and G. A. Somorjai, Nano Lett. **7**, 3097 (2007).
[29] V. Demers-Carpentier and P. H. McBreen, J. Phys. Chem. C **115**, 6513 (2011).
[30] M. Saeys, M.-F. Reyniers, G. B. Marin, and M. Neurock, J. Phys. Chem. B **106**, 7489 (2002).
[31] C. Morin, D. Simon, and P. Sautet, J. Phys. Chem. B **108**, 5653 (2004).
[32] V. Nieminen, K. Honkala, A. Taskinen, and Murzin, J. Phys. Chem. C **112**, 6822 (2008).
[33] J. M. Gottfried, E. K. Vestergaard, P. Bera, and C. T. Campbell, J. Phys. Chem. B **110**, 17539 (2006).
[34] L. Schimka, J. Harl, A. Stroppa, A. Grüneis, M. Marsman, F. Mittendorfer, and G. Kresse, Nature Mater. **9**, 741 (2010).
[35] T. R. Mattsson and A. E. Mattsson, Phys. Rev. B **66**, 214110+ (2002).
[36] J. L.F. Da Silva, C. Stampfl, and M. Scheffler, Surf. Sci. **600**, 703 (2006).
[37] See supplementary material at http://dx.doi.org/10.1063/1.4707952 for larger views of dimers and tables of frequencies.
[38] F. Delbecq, J. Catal. **152**, 217 (1995).
[39] F. Delbecq and P. Sautet, J. Catal. **211**, 398 (2002).
[40] D. Loffreda, F. Delbecq, F. Vigné, and P. Sautet, J. Am. Chem. Soc. **128**, 1316 (2006).
[41] F. Delbecq, D. Loffreda, and P. Sautet, J. Phys. Chem. Lett. **1**, 323 (2009).
[42] V. Demers-Carpentier, M.-A. Laliberté, Y. Pan, G. Mahieu, S. Lavoie, G. Goubert, B. Hammer, and P. H. McBreen, J. Phys. Chem. C **115**, 1355 (2010).
[43] T. Steiner, Chem. Commun. **1997**, 727.
[44] S. Mathieu and G. Trinquier, Phys. Chem. Chem. Phys. **11**, 8183 (2009).
[45] S. Lavoie and P. H. McBreen, J. Phys. Chem. B **109**, 11986 (2005).
[46] R. Vargas, J. Garza, D. A. Dixon, and B. P. Hay, J. Am. Chem. Soc. **122**, 4750 (2000).
[47] V. S. Bryantsev and B. P. Hay, Org. Lett. **7**, 5031 (2005).
[48] W. Gao, W. T. Zheng, and Q. Jiang, J. Chem. Phys. **129**, 164705 (2008).